Applied Catalysis B: Environmental 194 (2016) 202–208

Contents lists available at ScienceDirect

Applied Catalysis B: Environmental

journal homepage: www.elsevier.com/locate/apcatb

Efficient Pt-free electrocatalyst for oxygen reduction reaction: Highly ordered mesoporous N and S co-doped carbon with saccharin as single-source molecular precursor

Yongqi Hua [a], Tingting Jiang [a,1], Kun Wang [a], Mingmei Wu [a], Shuqin Song [a,*], Yi Wang [b,*], Panagiotis Tsiakaras [c,*]

[a] The Key Lab of Low-carbon Chemistry & Energy Conservation of Guangdong Province, School of Materials Science and Engineering, Sun Yat-sen University, Guangzhou 510275, China
[b] The Key Lab of Low-carbon Chemistry & Energy Conservation of Guangdong Province, School of Chemical Engineering and Technology, Sun Yat-sen University, Guangzhou 510275, China
[c] Laboratory of Alternative Energy Conversion Systems, Department of Mechanical Engineering, School of Engineering, University of Thessaly, Pedion Areos, 38834, Greece

ARTICLE INFO

Article history:
Received 1 March 2016
Received in revised form 20 April 2016
Accepted 27 April 2016
Available online 28 April 2016

Keywords:
Ordered mesoporous N and S co-doped carbon
Oxygen reduction reaction
Electrocatalytic activity
Methanol tolerance
Stability

ABSTRACT

Despite that nitrogen (N) and sulfur (S) co-doped ordered mesoporous carbon (OMC) as Pt-free catalyst for oxygen reduction reaction (ORR) shows a desirable performance, the synthesis method is always complicated and expensive, which greatly hinders its development and application. In the present work, a highly ordered mesoporous N and S co-doped carbon material is developed. The material is obtained by combining hard template and high-temperature pyrolysis method using cheap saccharin as a single-source molecular precursor, SBA-15 as the hard template and $FeCl_3$ as the catalyst to promote the carbonization process. It is found that the as-prepared SN-OMC catalyst, compared with the commonly used commercial Pt/C (20 wt.%), exhibits comparable ORR electrocatalytic activity with mainly four-electron ($4e^-$) process, superior stability and inertness to methanol in alkaline media, which could mainly benefit from the highly ordered mesoporous structure and the synergistic effect caused by the dual N and S doping. These advantages render SN-OMC a promising ORR electrocatalyst and a cheap alternative to Pt/C for practical fuel cell applications.

1. Introduction

Direct methanol fuel cells (DMFCs) have been the last two decades a hot issue as a kind of new type energy electrochemical converter with their simple structure, low-cost fuel (methanol), environmental benignity, high energy density, and high conversion rate [1,2]. On the other hand, there still exist some challenges for their real application and industrialization. Among them, the sluggish cathodic *oxygen reduction reaction* (ORR) is the main bottleneck [3,4]. Currently, Pt and Pt-based alloys are the typical and conventional catalysts for ORR with efficient electrocatalytic performance. However, Pt, as a noble metal, is not desirable for ORR catalyst considering its high-cost, scarce world reserves, poor stability and low anti-poison capability [5].

Great effort has been devoted to developing a new efficient, durable, and inexpensive ORR catalyst to decrease or even replace the usage of Pt. Prosperously, TM-N-C (TM = Fe, Co *etc.*) materials have been extensively considered as a promising alternative to Pt/C catalysts because of their excellent ORR electrocatalytic performance, but the opinions about their corresponding active sites are controversial. So far, there have been two different viewpoints: most of researchers insisted on that TM-N moieties were the active sites, while the others suggested that metal-free N-C moiety itself could efficiently catalyze the ORR process [6–8]. Until 2006, Ozkan et al. found that TM species were unnecessary for ORR, by providing the proof that N-doped carbon with less than 1 ppm metal contamination could also catalyze ORR in acidic electrolyte [9]. Next, Dai's group reported that N-doped carbon nanotube arrays showed a comparable ORR performance to the commercial Pt/C in alkaline media [10], which makes *metal-free ORR catalysts* (MFORCs)

* Corresponding authors.
E-mail addresses: stsssq@mail.sysu.edu.cn (S. Song), wangyi76@mail.sysu.edu.cn (Y. Wang), tsiak@uth.gr (P. Tsiakaras).
[1] Tingting Jiang made the same contribution as Yongqi Hua.

http://dx.doi.org/10.1016/j.apcatb.2016.04.056
0926-3373/

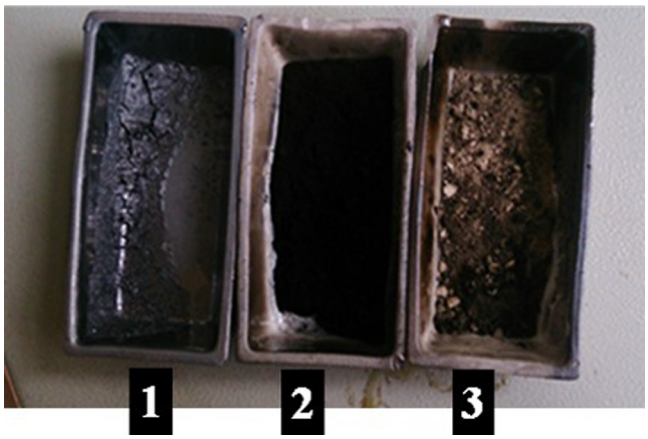

Fig. 1. Morphology of the three samples after carbonization (Sample 1: $FeCl_3{\cdot}6H_2O$ + Saccharin; Sample 2: $FeCl_3{\cdot}6H_2O$ + Saccharin + SBA-15; Sample 3: Saccharin + SBA-15).

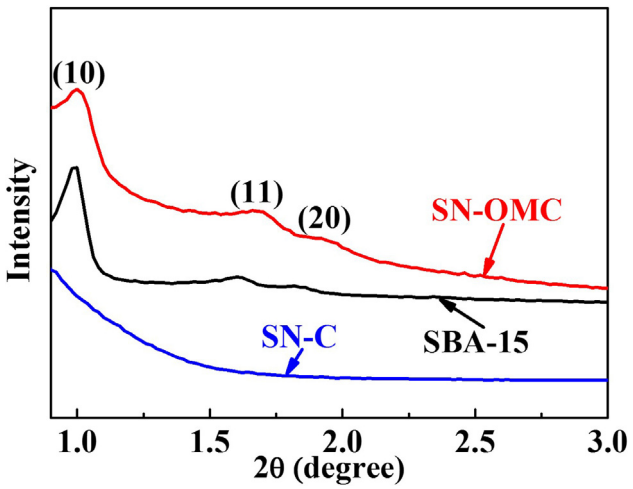

Fig. 2. Small angle X-ray diffraction patterns of SN-OMC, SN-C, and SBA-15 at a scan rate of 0.3° min^{-1}.

an important candidate to replace the commercial Pt/C. Recently, other non-metal elements besides N (*e.g.* B, P, S, F, and I) [11–32] have been introduced into carbon materials. Although a moderate ORR performance has been obtained on these materials, their ORR activity is still inferior to that of the state-of-the-art Pt/C catalysts. To make MFORCs truly competitive with Pt/C, two crucial factors governing the electrocatalytic performance of the MFORCs have to be simultaneously considered: (1) the intrinsic nature of active sites, which are determined by the doped heteroatoms and their synergistic effects; (2) the accessible part of active sites and the mass transfer properties of ORR-relevant species, which are determined by the structure of carbon materials [33–40]. With the above two features, some researchers have proposed to make heteroatoms co-doped porous carbon materials with big specific surface area as MFORCs. Qiao's group reported S and N co-doped mesoporous graphene to improve the ORR catalytic activity in basic media, owing to the synergistic effect from both the multiple-element doping and the big specific surface area [30]. Also, Dai's group proposed co-doped graphene, with B and N, showed desirable ORR catalytic activity, as the ORR activity was controlled not only by the increased number of doped heteroatoms but also by the synergistic effect between the dopants [41]. Additionally, Li's group revealed a new type of non-precious metal electrocatalysts, WN nanoparticles on simultaneously generated N-carbon black under ammonia annealing, which exhibited excellent ORR performance in basic media due to the synergistic effect between the WN and N-carbon black [45–47]. In spite of tremendous progress, the desirable MFORCs, which possess the above two features and thus achieve high ORR performance, have rarely been achieved.

Here we report a new type of Pt-free catalysts, S and N co-doped highly ordered mesoporous carbon (SN-OMC), which is synthesized by combining hard template and single molecule shear methods with (i) saccharin ($C_7H_5NO_3S$) as the precursors of N, S, and C (considering its wide application, mature production and low-cost), (ii) $FeCl_3$ as the catalyst to promote the carbonization, and (iii) SBA-15 as the hard template, respectively. Such a unique catalyst possesses the above mentioned crucial features for an excellent ORR performance, including highly effective intrinsic active sites (N-C and S-C), large specific surface area (743 $m^2\,g^{-1}$) and very highly ordered structure. Moreover, this method is simple, economical and easily scalable. Consequently, the electrocatalyst is able to efficiently catalyze a four-electron ORR process with comparable electrocatalytic activity and stability with respect to the commercial Pt/C catalyst (E-TEK) in alkaline electrolyte.

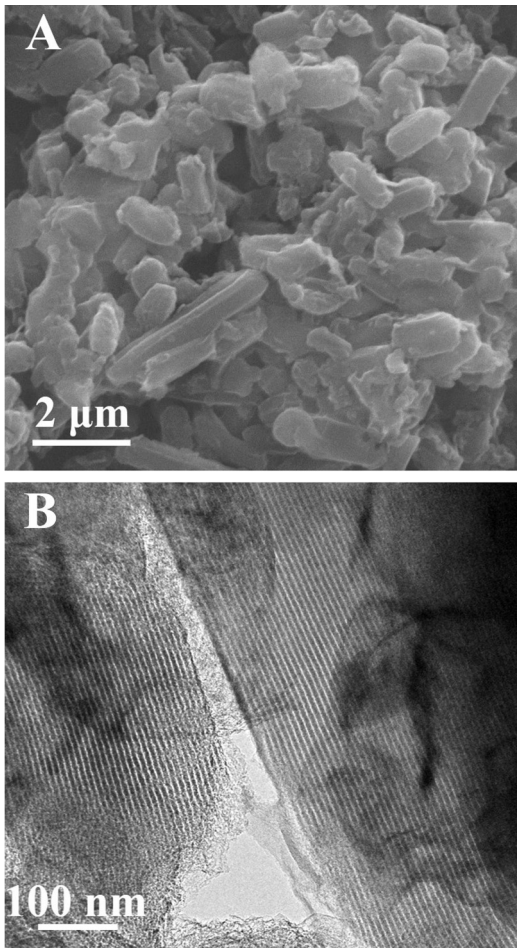

Fig. 3. SEM image (A) and TEM image (B) of SN-OMC.

2. Experimental

2.1. Raw materials

Saccharin and hexahydrate ferric chloride ($FeCl_3{\cdot}6H_2O$) were purchased from Aladdin (Shanghai, China). All the other used chemicals were of analytical reagent grade. Deionized water with specific

resistance more than 18.0 MΩ cm^{-1} was obtained by a water purification system.

2.2. Materials preparation

Ordered mesoporous silica materials (SBA-15) as the hard template (1.0 g) and $FeCl_3 \cdot 6H_2O$ as the catalyst for carbonization were uniformly dispersed in the mixture solution of ethanol and deionized water ($V_{ethanol}$:V_{water} = 4:1) by vigorous stirring and ultrasonication. Saccharin (3.0 g) was completely dissolved in the above uniform suspension. The mixture solution was evaporated into a yellow viscous liquid with stirring at 50 °C; then the sample was further dried in a vacuum oven at 50 °C for 12 h. The obtained powder was pyrolyzed at 800 °C in a tube furnace for 3 h at a heating rate of 1 °C min^{-1} from 50 °C to 800 °C in a flowing nitrogen atmosphere. The black powder was then placed in the HF solution (20 wt%) for 24 h to etch the SBA-15 hard template. The as-prepared carbon materials, denoted as SN-OMC, were obtained by washing and drying.

For the sake of comparison, the samples without $FeCl_3 \cdot 6H_2O$ or SBA-15 (denoted as SN-C) were also prepared under the same conditions.

2.3. Physico-chemical characterization

The *small angle X-ray powder diffraction* (SAXD) (Rigaku Co., Japan) was carried out with Cu Kα radiation (40 kV, 26 mA) at a scan rate of 0.3° min^{-1}. *Transmission electron microscopy* (TEM) and *scanning electron microscopy* (SEM) images were obtained with JEOL TEM-2010 and JSM-6330F instruments, respectively. Before the TEM and SEM measurements, the catalysts were dispersed in ethanol solution by ultrasonic water bath, and then dried onto the copper grids. The nitrogen adsorption/desorption experiments were performed on Micromeritics ASAP2020. Before the measurements, the samples were dried at 250 °C for more than 8 h under vacuum conditions. The specific surface area was calculated by using the *Brunauer-Emmett-Teller* (BET) analysis. *X-ray photoelectron spectroscopy* (XPS) measurements were tested on a VG Scientific ESCALAB250 instrument equipped with Al Kα X-ray source (1486.6 eV). The obtained spectrograms were analyzed with Xpspeak41 software.

2.4. Electrochemical measurements

2.4.1. Activity evaluation

2.4.1.1. Rotating disk electrode (RDE) measurements. The electrochemical measurements were carried out in an Auto84480 instrument equipped with a three-electrode cell having a Pt foil as the counter electrode. Ag/AgCl electrode (saturated KCl solution) was used as the reference electrode, which potential was −0.198 V [*vs.* NHE (normal hydrogen electrode)]. A *glassy carbon* (GC) disk with a diameter of 5.0 mm served as the substrate for the working electrode. The catalyst thin film attached on the GC disk electrode was used as the working electrode, which was prepared as follows: 7.0 mg of the catalyst sample (for non-Pt catalysts) was ultrasonically dispersed in the mixed solution of 350.0 μL ethanol and 95.0 μL Nafion® solution (5 wt.%) for 1 h, and then 5.0 μL of the above suspension was dropped onto the surface of the GC disk electrode. The catalyst loading was maintained at 400 μg catalyst cm^{-2}. For the commercial Pt/C (20 wt. Pt%, E-TEK), 5.0 mg of the sample was ultrasonically dispersed in the solution of 1.8 mL ethanol and 0.2 mL Nafion® solution (5 wt%) for 1 h, and 12 μL of the above obtained suspension was dropped onto the surface of the GC disk electrode with a catalyst loading of 30 μg Pt cm^{-2}.

The cyclic voltammetry (CV) tests were performed in N_2 or O_2-saturated 0.1 mol L^{-1} KOH solution with a scan rate of 10 mV s^{-1}.

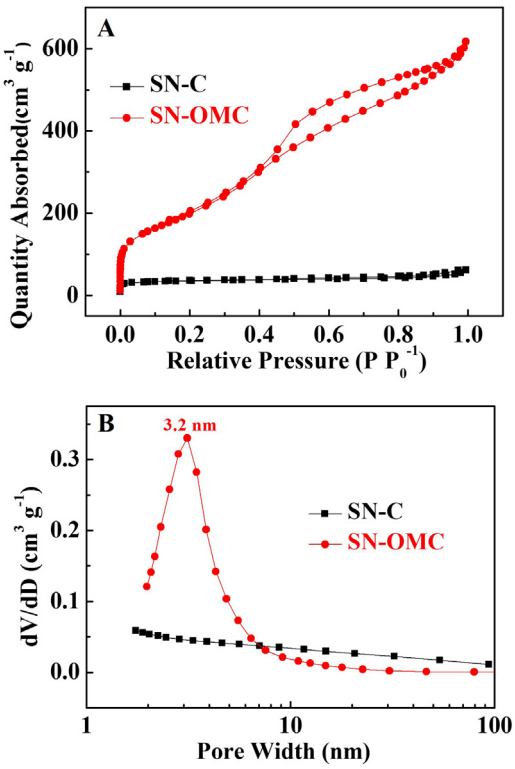

Fig. 4. N_2 adsorption-desorption isotherms (A) and pore size distribution (B) of SN-C and SN-OMC.

In the case of linear sweeping voltammetry, the working electrode was scanned at a rate of 10 mV s^{-1} with the rotating speed from 400 to 2000 rpm. The activity for ORR was evaluated in N_2 or O_2-saturated 0.1 mol L^{-1} KOH solution at room temperature.

To investigate the ORR mechanism, Koutecky-Levich plots were analyzed at various electrode potentials. The slopes of their linear fitting were used to calculate the number of transferred electrons (n) in the ORR process on the basis of the Koutecky-Levich equation:

$$i^{-1} = i_k^{-1} + i_L^{-1} \quad (1)$$

$$i_L = 0.620nFAD_O{}^{2/3}\omega^{1/2}\nu^{-1/6}C_{O_2} = B\omega^{1/2} \quad (2)$$

where i_L (A) is the limiting current under diffusion control, i_k (A) the kinetic current of the reaction with active substance on the electrode surface, n (mol) the transferred electrons when each O_2 molecule is reduced, F the Faraday's constant (96485C mol^{-1}), A (cm^2) the geometric area of the electrode, D_{O2} (cm^2 s^{-1}) the diffusion coefficient of O_2 in O_2-saturated 0.1 mol L^{-1} KOH solution, ω (s) the electrode rotating speed in rpm, ν (cm^2 s^{-1}) the kinematic viscosity of the electrolyte, C_{O_2} (mol cm^{-3}) the O_2-staturated concentration in O_2-saturated 0.1 mol L^{-1} KOH solution and B (mA $rpm^{-1/2}$) the reciprocal of the slopes [26].

2.4.1.2. Rotating ring-disk electrode (RRDE) measurements. The catalysts and electrodes were prepared through the same procedure described above. The ring current (I_R) was measured with a Pt ring electrode. Pt ring electrode was polarized at 0.5 V (*vs.* Ag/AgCl) in O_2-saturated 0.1 mol L^{-1} KOH solution. The four-electron selectivity of ORR at the catalyst was calculated based on Eq. (3). The H_2O_2 yield was determined by Eq. (4).

$$n = \frac{4 \times I_D}{I_D + I_R/N} \quad (3)$$

$$\%HO_2^- = \frac{4 - n}{2} \quad (4)$$

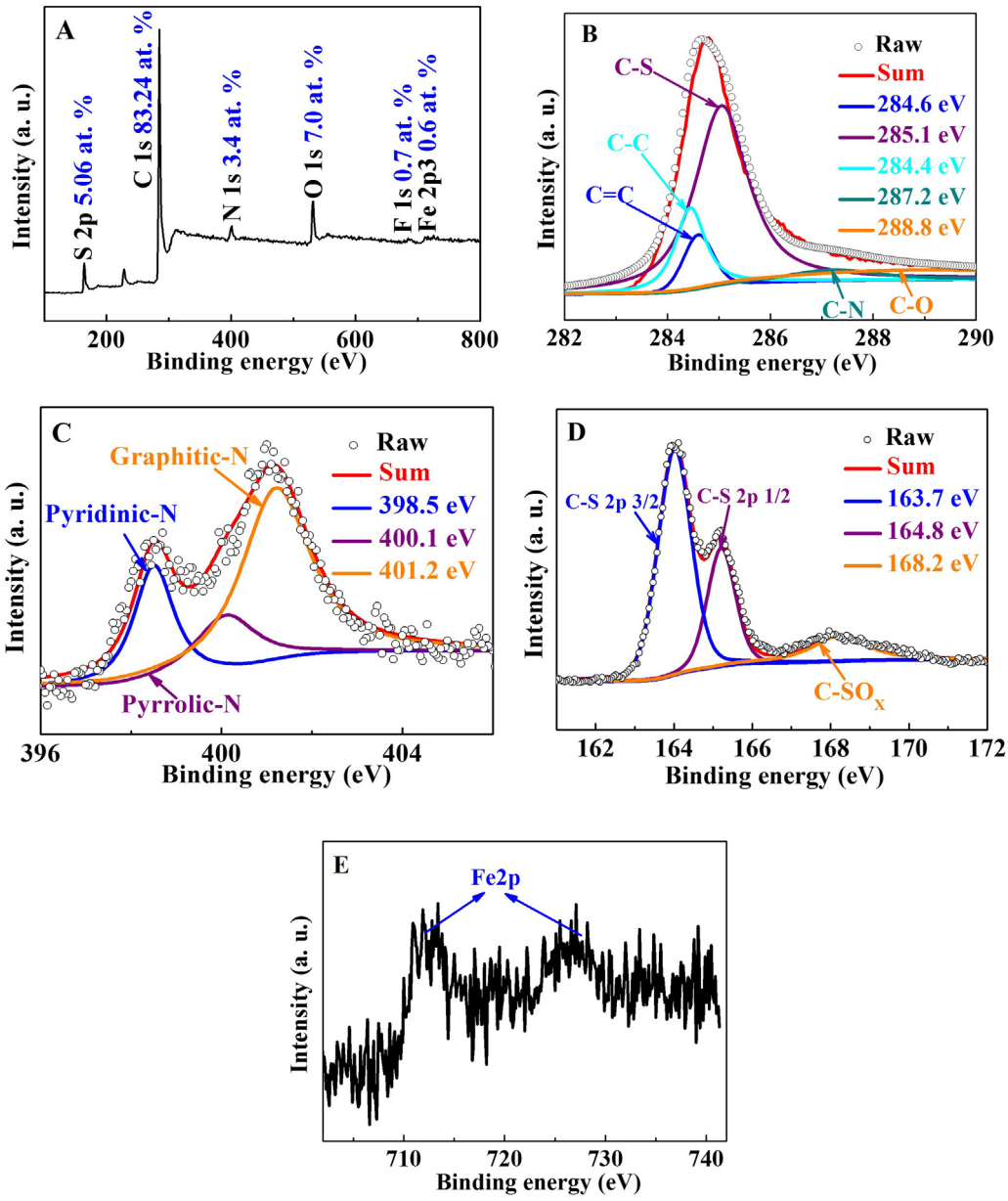

Fig. 5. XPS survey of SN-OMC (A); the high-resolution C1s XPS spectrum (B); the high-resolution N1s XPS spectrum (C); The high-resolution S2p XPS spectrum (D); Fe 2p scan of SN-OMC (E).

where I_D is the disk current, I_R the ring current, and N the H_2O_2 collection efficiency of the Pt ring with a value of 0.37 [40].

2.4.2. Tolerance and stability tests

The methanol tolerance test was carried out in O_2-saturated 0.1 mol L^{-1} KOH solution with or without 0.5 mol L^{-1} CH_3OH by using the CV technique. The accelerated aging tests were performed in O_2-saturated 0.1 mol L^{-1} KOH solution also by the aid of the CV technique. The accelerated aging was obtained by 10,000 potential cycles between 0.6 V–1.0 V (*vs.* NHE) at a rate of 50 mV s^{-1}.

3. Results and discussion

Saccharin ($C_7H_5NO_3S$) containing N, S, and C, was adopted as the precursors to synthesize N and S codoped carbon through the single molecule shear method. The effect of the hard template (SBA-15) and the carbonization catalyst ($FeCl_3$) on the sample can be easily judged from the extrinsic feature of samples. The pictures of the obtained three samples are seen in Fig. 1. By comparing them, one can intuitively find that by introducing the SBA-15 hard template, the sample becomes lighter (Samples 2 and 3), meaning a lower density and more pores. Meanwhile, the color of the sample without adding $FeCl_3$ (sample 3) is obviously lighter than that of the other two samples, indicating that $FeCl_3{\cdot}6H_2O$ can promote the carbonization process. It should be noted that after etching of the SBA-15 template there was a little carbon residue left for Sample 3. Hence, considering the poor carbonization and thus lower electrical conductivity, Sample 3 will not be involved in the following discussion.

The small-angle XRD patterns of SBA-15, SN-OMC, and SN-C are given in Fig. 2. The 2θ peaks at 0.998, 1.663, and 1.940° of SBA-15 stand for the diffraction peaks of (10), (11) and (20) of two dimensional hexagonal structure, respectively. Similarly, the patterns of the as-prepared SN-OMC also show these three corresponding typical diffraction peaks, indicating the reverse replica structure of

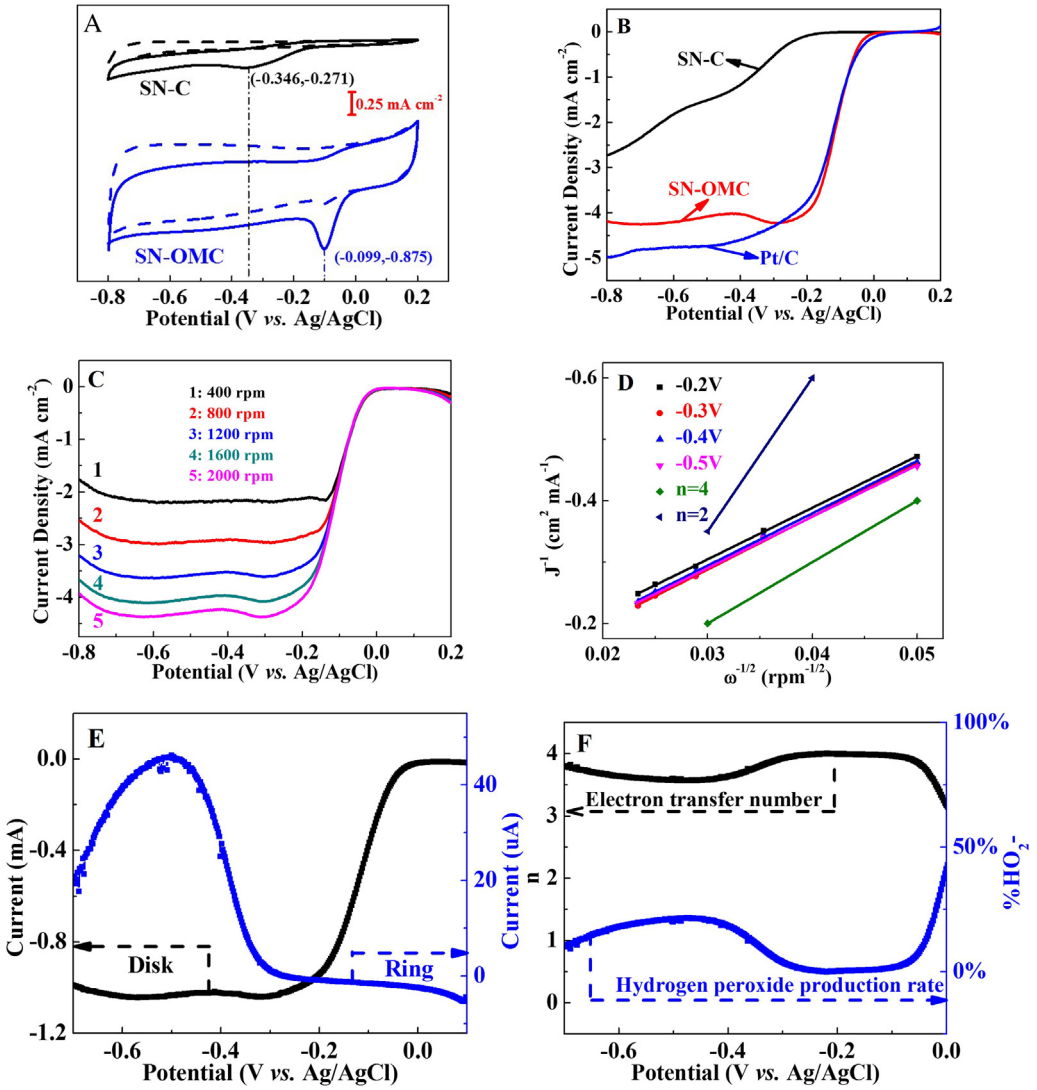

Fig. 6. CV curves of SN-C, SN-OMC in N_2 (dash line) and O_2-(solid line) saturated 0.1 mol L^{-1} KOH solution at a scan rate of 10 mV s^{-1} (A); RDE voltammograms in an O_2-saturated 0.1 mol L^{-1} KOH solution at room temperature (rotation speed: 1600 rpm, scan rate: 10 mV s^{-1}) for SN-C, SN-OMC, and commercial Pt/C (B); RDE voltammograms for SN-OMC at various rotation speeds (scan rate: 10 mV s^{-1}) (C) and the Koutecky-Levich plots at different potentials (D) in an O_2-saturated 0.1 mol L^{-1} KOH solution; RRDE voltammograms in an O_2-saturated 0.1 mol L^{-1} KOH solution at room temperature (rotation speed: 1600 rpm, scan rate: 10 mV s^{-1}) for SN-OMC (E); Electron transfer number and hydrogen peroxide yield obtained from the RRDE curves for SN-OMC (F).

SN-OMC. While, for the patterns of SN-C, there is no any diffraction peak, indicating a disordered pore structure.

In order to better observe the morphology of the as-prepared SN-OMC, SEM and TEM micrographs were also obtained. From the SEM image shown in Fig. 3A, the hexagonal structure rodlike particles are clearly observed, possessing a typical structure of SBA-15 [42–44], with a length of *ca.* 1 μm. A highly ordered 2D hexagonal mesostructure of the SN-OMC can also be verified by the parallel arranged channels from the TEM image of SN-OMC (Fig. 3B).

In order to further investigate the pore structure of the samples (SN-C and SN-OMC), the N_2 adsorption-desorption isotherms of samples were recorded (Fig. 4). Typical IV nitrogen adsorption/desorption isotherms with distinct hysteretic loops indicate the mesoporous structure of the SN-OMC (Fig. 4A). The mesopore size distribution is centered at 3.2 nm (Fig. 4B). Comparatively, the overlapping N_2 adsorption/desorption isotherms of the SN-C reveal the nonporous structure. The corresponding *Brunauer-Emmett-Teller* (BET) surface areas of these two samples are 743 $m^2 g^{-1}$ (SN-OMC) and 120 $m^2 g^{-1}$ (SN-C). In other words, the SN-OMC exhibits the ordered mesoporous structure with big specific surface area. Such features are favorable for active sites exposure and the rapid mass transfer of the ORR-relevant species.

The XPS results show the surface atomic percentages of C (83.24 at.%), O (7.0 at.%), S (5.06 at.%), N (3.4 at.%), and Fe (0.6 at.%) for the SN-OMC catalyst (Fig. 5A). This result confirms that N and S atoms have been successfully incorporated into the carbon framework. High resolution XPS was performed to further investigate the bonding configurations in SN-OMC. As shown in Fig. 5B, the C1s spectrum displays an asymmetric shape with the peak energy of 284.78 eV and the peak can be deconvoluted into five C species. They are corresponding to C═C (284.6 eV), C—S (285.1 eV), C—C (284.4 eV), C—N (287.2 eV), and C—O (288.8 eV) [30,40], which confirms once again that N and S are simultaneously doped into the carbon framework. The high resolution N1s spectrum (Fig. 5C) can be assigned into three N species, corresponding to pyridinic-N (398.5 eV), pyrrolic-N (400.1 eV), and graphitic-N (401.3 eV) [30], respectively, further confirming the presence of three types of N species in the carbon framework. Remarkably, the pyridinic-N (23.1 at.%), pyrrolic-N (17.4 at.%), and graphitic-N (59.5 at.%) are recognized as ORR active species [37]. The Fe2p spectrum (Fig. 5E)

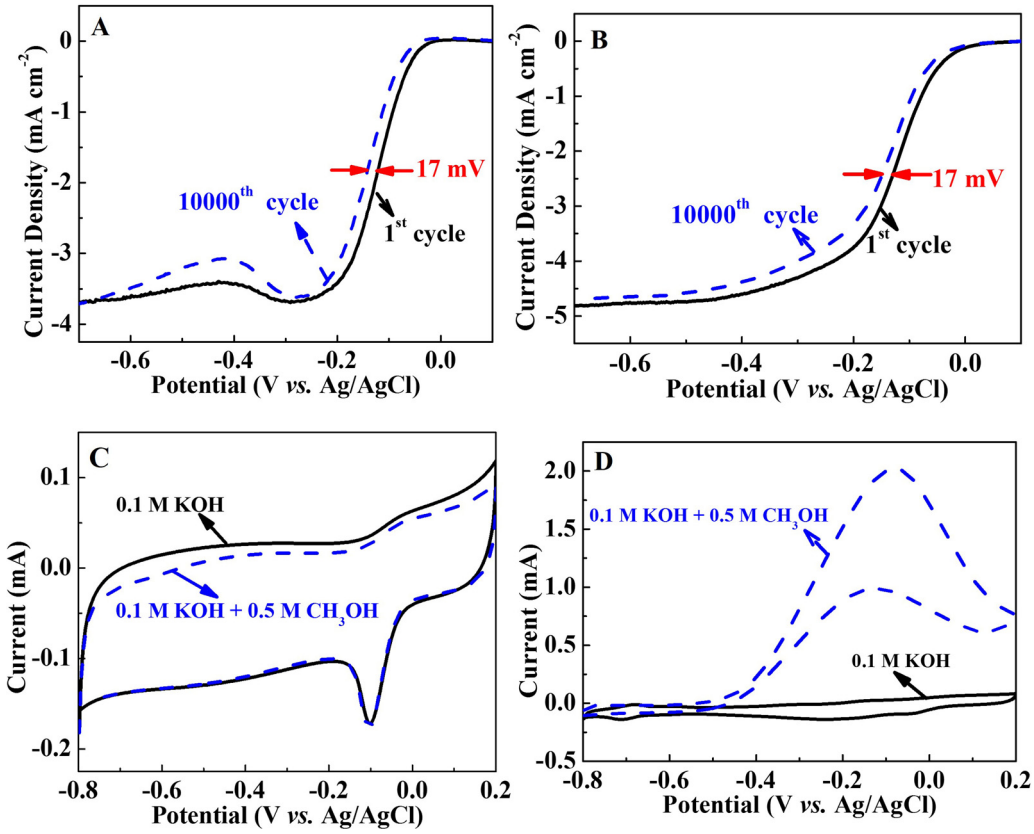

Fig. 7. RDE voltammograms of SN-OMC (A) and commercial Pt/C (B) before and after 10,000 cycles between 0.6 V–1.0 V (*vs.* NHE) at 50 mV s^{-1} in an O_2-saturated 0.1 mol L^{-1} KOH solution; Cyclic voltammograms of SN-OMC (C) and commercial Pt/C (D) in an O_2-saturated 0.1 mol L^{-1} KOH solution at room temperature with and without 0.5 mol L^{-1} CH_3OH.

shows peaks of Fe2p1/2 and Fe2p3/2 of oxidized Fe species [48,49]. Similarly, a detailed scan of S2p spectrum (Fig. 5D) can be fitted into three peaks: two of them at 163.7 eV and 164.8 eV are assigned to thiophene-S (-C-S-C-) owing to the spin-orbit coupling, and the intense peak at 168.2 eV corresponds to oxidized-S (-C-SO_x-C-). The thiophene-S indicates that the incorporated S atoms are mainly bonded with two C atoms at the edges and defects of ordered mesoporous carbon, which are chemically active for ORR [25]. These results indicated that saccharin could be used as the single source to synthesize N and S co-doped carbon materials.

To evaluate the ORR catalytic activity of the SN-OMC in alkaline media, its electrocatalytic properties were firstly examined in N_2 or O_2-saturated 0.1 mol L^{-1} KOH solution using the CV technique at a scan rate of 10 mV s^{-1}. For comparison, SN-C was also measured at the same experimental conditions and the results are depicted in Fig. 6A. In the N_2-saturated solution, all materials deliver featureless CV curves, while they present well-defined ORR reduction peaks in O_2-saturated 0.1 mol L^{-1} KOH solution. Comparatively, the CV curve for the SN-OMC shows a distinct reduction peak at −0.099 V, corresponding to the ORR. It is clear that the onset potential for ORR significantly shifts to the positive direction relative to that of the SN-C. The ORR activities of these catalysts were further investigated by LSV polarization curves (Fig. 6B). In accordance with the CV results, SN-OMC exhibits a better electrocatalytic activity with a more positive onset reduction potential (−0.005 V) and limiting current density (−4.2 mA cm^{-2}) than the corresponding values (−0.185 V, −2.7 mA cm^{-2}) of the SN-C. This could be attributed to the highly ordered mesoporous structure and the synergistic effect caused by dual N and S doping. More to the point, the SN-OMC shows a comparable ORR activity to the commercial Pt/C in alkaline media.

For a further insight into the ORR kinetics of the SN-OMC in alkaline media, a set of polarization curves were recorded on the RDE at different rotating speeds (Fig. 6C). The linearity of the Koutecky-Levich plots and near parallelism of the fitting lines to the theoretical 4e⁻ line (Fig. 6D) suggests a first-order reaction kinetics towards the concentration of the dissolved O_2 and similar electron transfer number (4e⁻) for ORR at different potentials. To verify the ORR catalytic pathway at SN-OMC, the RRDE technique has been adopted in order that the amount of H_2O_2 generated at the disk electrode can be accurately determined by the ring electrode. In the potential range of −0.7 V to 0 V, the measured values of H_2O_2 yield are below ~25%, giving an electron transfer number of ~4.0 (Figs. 6E and 6F). This is consistent with the results obtained from the Koutecky-Levich plots based on RDE measurements, indicating that the ORR follows a four-electron path at SN-OMC in alkaline media.

The durability of the SN-OMC catalyst was assessed using the accelerated durability test protocol of the US Department of the Energy by cycling the catalysts between 0.6 V and 1.0 V (*vs.* NHE) at 50 mV s^{-1} under O_2 atmosphere. As it can be seen from Fig. 7A, after 10,000 continuous potential cycles, the half-wave potential $E_{1/2}$ exhibits a small negative shift of ~17 mV at the SN-OMC catalyst, which is almost the same as that at the commercial Pt/C catalyst (~17 mV; see Fig. 7B). The as prepared SN-OMC catalyst was also exposed to fuel molecules for testing the poisoning effects. For DMFCs, it is highly desirable that ORR catalysts exhibit high tolerance to methanol that can pass across the electrolyte membrane from the anode to the cathode (methanol crossover). The CV curves depicted in Figs. 7C and 7D were obtained in the presence of 0.5 mol L^{-1} methanol in O_2 saturated 0.1 mol L^{-1} KOH solution. A drastic decrease in the ORR activity at Pt/C, due to the simultane-

ous methanol oxidation, is observed; in comparison, the SN-OMC catalyst shows almost no activity loss. The excellent tolerance to methanol poisoning effect can be attributed to its much lower ORR potential than that required for methanol oxidation. The above results suggest that the SN-OMC can be used as a promising alternative Pt-free ORR catalyst with desirable activity, excellent durability and desirable methanol tolerance in alkaline media.

4. Conclusion

In the present work, a novel technique, by combing hard template and single molecule shear method, has been developed for the synthesis of highly ordered mesoporous SN-OMC. The entire synthesis process is very simple, economical, and scalable. The catalyst ($FeCl_3$) and template (SBA-15) are both necessary for the structure construction and performance enhancement of the as-prepared SN-OMC catalyst. The ORR activity and stability of the obtained SN-OMC is comparable to that of the commercial Pt/C in alkaline media. Meanwhile, SN-OMC exhibits high $4e^-$ selectivity for ORR, and better methanol tolerance than does the state-of-the-art Pt/C catalyst. Additionally, the present work may inspire researchers in the fields of energy conversion and storage, and catalysis to develop more techniques for hetero-elements co-doped mesostructure carbon synthesis.

Acknowledgements

Authors are grateful to the National Natural Science Foundation of China (No. 21576300, 21575299, 21276290), the Sino-Greek Science and Technology Cooperation Project (2013DFG62590), and the Guangdong Province Nature Science Foundation (2014A030313150) for financial support.

References

[1] A.S. Aricò, S. Srinivasan, V. Antonucci, Fuel Cells 1 (2001) 133–161.
[2] S. Song, V. Maragou, P. Tsiakaras, J. Fuel Cell Sci. Technol. 4 (2007) 203–209.
[3] J.M. Noël, A. Latus, C. Lagrost, E. Volanschi, P. Hapiot, J. Am. Chem. Soc. 134 (2012) 2835–2841.
[4] C.C.M. Neumann, E. Laborda, K. Tschulik, K.R. Ward, R.G. Compton, Nano Res. 6 (2013) 511–524.
[5] T. Jiang, L. Yan, Y. Meng, M. Xiao, Z. Wu, P. Tsiakaras, S. Song, Appl. Catal. B: Environ. 162 (2015) 275–281.
[6] K. Wan, G.F. Long, M.Y. Liu, L. Du, Z.X. Liang, P. Tsiakaras, Appl. Catal. B: Environ. 165 (2015) 566–571.
[7] A.G. Saputro, H. Kasai, Phys. Chem. Chem. Phys. 17 (2015) 3059–3071.
[8] H.M. Barkholtz, L. Chong, Z.B. Kaiser, T. Xu, D.J. Liu, Catalysts 5 (2015) 955–965.
[9] P.H. Matter, U.S. Ozkan, Catal. Lett. 109 (2006) 115–123.
[10] K. Gong, F. Du, Z. Xia, M. Durstock, L. Dai, Science 323 (2009) 760–764.
[11] Y. Wang, Y. Shao, D.W. Matson, J. Li, Y. Lin, ACS Nano 4 (2010) 1790–1798.
[12] M. Zhang, L. Dai, Nano Energy 1 (2012) 514–517.
[13] L. Zhang, Z. Xia, J. Phys. Chem. C 115 (2011) 11170–11176.
[14] Z.H. Sheng, H.L. Gao, W.J. Bao, F.B. Wang, X.H. Xia, J. Mater. Chem. 22 (2012) 390–395.
[15] J. Jin, F. Pan, L. Jiang, X. Fu, A. Liang, Z. Wei, J. Zhang, G. Sun, ACS Nano 8 (2014) 3313–3321.
[16] Y. Zhao, L. Yang, S. Chen, X. Wang, Y. Ma, Q. Wu, Y. Jiang, W. Qian, Z. Hu, J. Am. Chem. Soc. 135 (2013) 1201–1204.
[17] L. Ferrighi, M. Datteo, C.D. Valentin, J. Phys. Chem. C 118 (2013) 223–230.
[18] D.S. Yang, D. Bhattacharjya, M.Y. Song, J.S. Yu, Carbon 67 (2014) 736–743.
[19] R. Li, Z. Wei, X. Gou, W. Xu, RSC Adv. 3 (2013) 9978–9984.
[20] J. Wu, Z. Yang, Z. Wang, Q. Sun, R. Yang, Electrochem. Commun. 42 (2014) 46–49.
[21] U.B. Nasini, V.G. Bairi, S.K. Ramasahayam, S.E. Bourdo, T. Viswanathan, A.U. Shaikh, ChemElectroChem 1 (2013) 573–579.
[22] X. Chen, X. Chen, X. Xu, Z. Yang, Z. Liu, L. Zhang, X. Xu, Y. Chen, S. Huang, Nanoscale 6 (2014) 13740–13747.
[23] C. Dominguez, F.J. Pérez-Alonso, S.A. Al-Thabaiti, S.N. Basahel, A.Y. Obaid, A.O. Alyoubi, J.L.G. Fuente, S. Rojas, Electrochim. Acta 157 (2015) 158–165.
[24] Z. Yang, Z. Yao, G. Li, G. Fang, H. Nie, Z. Liu, X. Zhou, X. Chen, S. Huang, ACS Nano 6 (2012) 205–211.
[25] S. Inamdar, H.S. Choi, P. Wang, M.Y. Song, J.S. Yu, Electrochem. Commun. 30 (2013) 9–12.
[26] W. Wei, H. Liang, K. Parvez, X. Zhuang, X. Feng, K. Mullen, Angew. Chem. Int. Ed. 53 (2014) 1570–1574.
[27] X. Sun, Y. Zhang, P. Song, J. Pan, L. Zhuang, W. Xu, W. Xing, ACS Catal. 3 (2013) 1726–1729.
[28] H. Wang, A. Kong, Mater. Lett. 136 (2014) 384–387.
[29] J. Liu, P. Song, Z. Ning, W. Xu, Electrocatalysis 6 (2015) 132–147.
[30] J. Liang, Y. Jiao, M. Jaroniec, S.Z. Qiao, Angew. Chem. Int. Ed. 51 (2012) 11496–11500.
[31] Z. Yao, H. Nie, Z. Yang, X. Zhou, Z. Liu, S. Huang, Chem. Commun. 48 (2012) 1027–1029.
[32] L. Yang, S. Jiang, Y. Zhao, L. Zhu, S. Chen, X. Wang, Q. Wu, J. Ma, Y. Ma, Z. Hu, Angew. Chem. Int. Ed. 50 (2011) 7132–7135.
[33] Q. Shi, Y. Lei, Y. Wang, H. Wang, L. Jiang, H. Yuan, D. Fang, N. Wu, Y. Gou, Curr. Appl. Phys. 15 (2015) 1606–1614.
[34] Y. Zhan, J. Huang, Z. Lin, X. Yu, D. Zeng, X. Zhang, F. Xie, W. Zhang, J. Chen, H. Meng, Carbon 95 (2015) 930–939.
[35] J. Zhao, Z. Chen, J. Phys. Chem. C 119 (2015) 26348–26354.
[36] Y. Sun, J. Wu, H. Tian, J. Chao, R. Yang, Electrochim. Acta 178 (2015) 806–812.
[37] J. Chen, H. Zhang, P. Liu, G. Li, T. An, H. Zhao, Carbon 92 (2015) 339–347.
[38] S. Dou, A. Shen, Z. Ma, J. Wu, L. Tao, S. Wang, J. Electroanal. Chem. 753 (2015) 21–27.
[39] Y. Zhu, Y. Lin, B. Zhang, J. Rong, B. Zong, D. Su, ChemCatChem 7 (2015) 2840–2845.
[40] S. Gao, L. Li, K. Geng, X. Wei, S. Zhang, Nano Energy 16 (2015) 408–418.
[41] S. Wang, E. Iyyamperumal, A. Roy, Y. Xue, D. Yu, L. Dai, Angew. Chem. Int. Ed. 50 (2011) 11756–11760.
[42] M. Kruk, M. Jaroniec, C.H. Ko, R. Ryoo, Chem. Mater. 12 (2000) 1961–1968.
[43] M. Imperor-Clerc, P. Davidson, A. Davidson, J. Am. Chem. Soc. 122 (2000) 11925–11933.
[44] Y.M. Liu, Y. Cao, N. Yi, W.L. Feng, W.L. Dai, S.R. Yan, H.Y. He, K.N. Fan, J. Catal. 224 (2004) 417–428.
[45] M. Sun, H. Liu, Y. Liu, J. Qu, J. Li, Nanoscale 7 (2015) 1250–1269.
[46] Y. Dong, J. Li, Chem. Commun. 51 (2015) 572–575.
[47] Z. Wen, J. Liu, J. Li, Adv. Mater. 20 (2008) 743–747.
[48] M. Lefèvre, E. Proietti, F. Jaouen, J.P. Dodelet, Science 324 (2009) 71–74.
[49] C. Ma, E. Rangasamy, C. Liang, J. Sakamoto, K.L. More, M. Chi, Angew. Chem. Int. Ed. 54 (2015) 1–6.